AIP Journal of Applied Physics

Dipole coupling and dual Fano resonances in a silicon nanodimer

Zhi-Yong Jia, Jing-Ning Li, Hong-Wei Wu, Cheng Wang, Tian-Yong Chen, Ru-Wen Peng, and Mu Wang

Citation: Journal of Applied Physics **119**, 074302 (2016); doi: 10.1063/1.4941740
View online: http://dx.doi.org/10.1063/1.4941740
View Table of Contents: http://scitation.aip.org/content/aip/journal/jap/119/7?ver=pdfcov
Published by the AIP Publishing

JOURNAL OF APPLIED PHYSICS **119**, 074302 (2016)

Dipole coupling and dual Fano resonances in a silicon nanodimer

Zhi-Yong Jia, Jing-Ning Li, Hong-Wei Wu, Cheng Wang, Tian-Yong Chen, Ru-Wen Peng,[a] and Mu Wang

National Laboratory of Solid State Microstructures and School of Physics, Collaborative Innovation Center of Advanced Microstructures, Nanjing University, Nanjing 210093, China

(Received 27 December 2015; accepted 29 January 2016; published online 17 February 2016)

We demonstrate theoretically in this work the existence of dual Fano resonances in a silicon nanodimer, which result from the strong coupling between the magnetic dipole in one nanocylinder and the electric dipole in another. It is shown that the intensities of the Fano resonances can be controlled by changing the polarization of the incident light, and the wavelengths of the resonances can be shifted by varying the separation of nanocylinders. And a broadband scattering response is also presented. These results concerning the ohmic loss-less, easily fabricated silicon nanodimer may have promising applications in wave filters, solar cells, biosensing, etc. © *2016 AIP Publishing LLC*. [http://dx.doi.org/10.1063/1.4941740]

I. INTRODUCTION

Fano resonance[1] was originally introduced in atomic physics to describe the asymmetrical ionization spectral lines of certain atoms. Recently, with the development of nanoscience and nanotechnology, considerable attention has been paid to the Fano resonances in the metallic nanosystem,[2–4] which is a classical analogue to the well-known phenomenon of Fano resonance in atomic physics. The plasmonic Fano resonance has extremely narrow linewidth owing to the coupling between the broad bright resonance mode and the narrow dark mode that are supported by the metal nanostructures.[5–7] Various structures have been designed to achieve Fano resonances, such as metallic split rings,[8,9] metallic rod-shaped nanoantennas,[10] nanoclusters,[11,12] nanoshells,[13–15] and heterodimer structures.[16] This unique line shape, which is sensitive to geometry of the structure and the local environment, has great potential in applications related to biosensors,[17] light-slowing devices,[18] and plasmonic lasing.[19] However, the plasmonic nanostructures, which are fabricated using noble metals such as Ag or Au,[20] suffer from intrinsic losses at optical frequencies. This drawback affects the possible practical use of Fano resonance. In order to mitigate these losses in plasmonic structures, the structures of the metal-semiconductor,[21] metal-dielectric,[22] even superconductive materials[23] have been proposed to achieve Fano resonance.

Recently, dielectric nanoparticles with high refractive indices (in contrast to metallic nanoparticles) have been proposed to achieve optical resonance[24] in order to overcome the ohmic loss. Nevertheless, the high-index dielectric nanoparticles not only exhibit electric resonance as with the metallic nanoparticles but also exhibit magnetic resonance, which originates from the excited circular displacement current of the electric field inside the dielectric nanoparticle within the visible and infrared regimes.[25,26] When the nanoparticles become closer, the interactions between the high-index dielectric nanoparticles have been shown to induce hybridized modes, which can be used to achieve electromagnetic field enhancement.[27,28] In particular, a Fano resonance has also been observed in all-dielectric oligomers[29–33] and all-dielectric nanodimers[34] in the visible light regime, which originates from the coupling between the optically induced magnetic dipole mode of individual nanoparticles and the collective mode of the nanoparticle structure or the electric dipole mode in the gap of the nanodimer.

One may naturally ask whether multiple Fano resonances may occur in high-index dielectric nanostructures. It has been found that a single Si cylinder exhibits electric or magnetic dipole modes under different wavelengths of incident light.[35–37] By precisely tuning the interaction between the electric and magnetic dipole modes, here we propose a scheme to generate dual Fano resonances in a loss-less, easily fabricated Si nanodimer that consists of two nanocylinders.

In this work, we theoretically investigate the optical scattering of the Si cylindrical nanodimer mainly by using finite-difference time-domain (FDTD) simulations. On the basis of these simulations, dual Fano resonances are found in a Si nanodimer within the infrared light regime; these originate from the strong interaction between the electric dipole in one cylinder and the magnetic dipole in the other, which can be excited by incident light. We also investigate how the polarization of the incident light and the gap size of the nanodimer affect the dual Fano resonances and the scattering properties of the Si nanocylinders. The results show that the Fano resonance peaks become weak as the polarization of the incident light is tuned from 0° to 90°; moreover, the Fano resonance peaks redshift as the gap distance increases between the two nanocylinders. Interestingly, when the polarization of the incident light is tuned to 90°, a new Fano resonance peak emerges in the scattering spectrum owing to the coupling between the magnetic dipole mode in one cylinder and the magnetic hybrid mode in the other. Finally, a broadband and tunable scattering response that originates

[a]Author to whom correspondence should be addressed. Electronic mail: rwpeng@nju.edu.cn

from the interaction of electric-magnetic and magnetic-magnetic modes between the dimeric Si nanocylinders is shown in the scattering spectrum of the nanodimer. These results may potentially be applied in nanoantennas and Si-based solar cell devices.[38,39]

II. THEORETICAL MODEL

We start by examining the scattering spectrum of a single Si nanocylinder. It is well known that a single Si particle exhibits electric or magnetic dipole modes under incident light of different wavelengths. By means of FDTD simulations, we obtain the scattering spectra of the single Si cylinder with various diameters ranging from 220 nm to 400 nm, as shown in Fig. 1(a). When the diameter is set to 220 nm, there are two resonance peaks in the spectrum located at 760 nm and 970 nm. The peak at 970 nm corresponds to a magnetic dipole mode localized in the block of the cylinder, whereas the peak at 760 nm corresponds to an electric dipole mode; these findings are similar to the results in Refs. 37 and 38. Upon increasing the diameter of the Si nanocylinder, we see that both peaks redshift, and new peaks emerge in the short-wavelength region of the scattering spectrum. For example, a new electromagnetic mode of the Si cylinder emerges at a wavelength of 800 nm upon increasing the diameter to 300 nm.

The exact shifts of electric and magnetic dipole resonances of Si disks, which have been experimentally demonstrated,[40] can be achieved by employing the multipole expansion technique.[41] Yet we can find in the FDTD simulations that by carefully choosing the cylinder diameter, the magnetic dipole in one nanocylinder, and the electric dipole in another can appear at the almost same wavelength (as shown in Figs. 1(b) and 1(c)). Considering that the magnetic dipole in this system is an effective one, which essentially similar to an electric quadrupole (for example, to see the electromagnetic field distributions in Fig. 1(c)), the magnetic dipole and the electric dipole may couple each other.

Next, we consider a Si dimer that contains two nanocylinders with different diameters, and with the same height (240 nm) as shown in Fig. 2. In this case, the linearly polarized light is normally incident onto the system from the top surface of the nanodimer. The orientation of the light (k direction) and the polarization (with angle θ relative to the horizontal axis) are illustrated by the blue and black arrows, respectively. The thinner orange waves with blue arrows around the green box represent the scattered light. When the two cylinders become closer, the interaction between the electric dipole in one cylinder and the magnetic dipole in the other occurs in the system.

In the long-wavelength limit, when the characteristic size of the Si nanoparticle is considerably smaller than the incident wavelength, and the resulting optical resonance can be described by the effective electric and magnetic dipoles as below

$$\mathbf{p} = \varepsilon_0 \alpha_E \mathbf{E}_0, \quad \mathbf{m} = \chi_H \mathbf{H}_0, \tag{1}$$

where $\mathbf{p}$ and $\mathbf{m}$ denote the induced electric and magnetic dipoles, respectively; α_E and χ_H denote the electric and magnetic polarizabilities, respectively; $\mathbf{E}_0$ and $\mathbf{H}_0$ denote the incident fields; and ε_0 denotes the electric permittivity. It

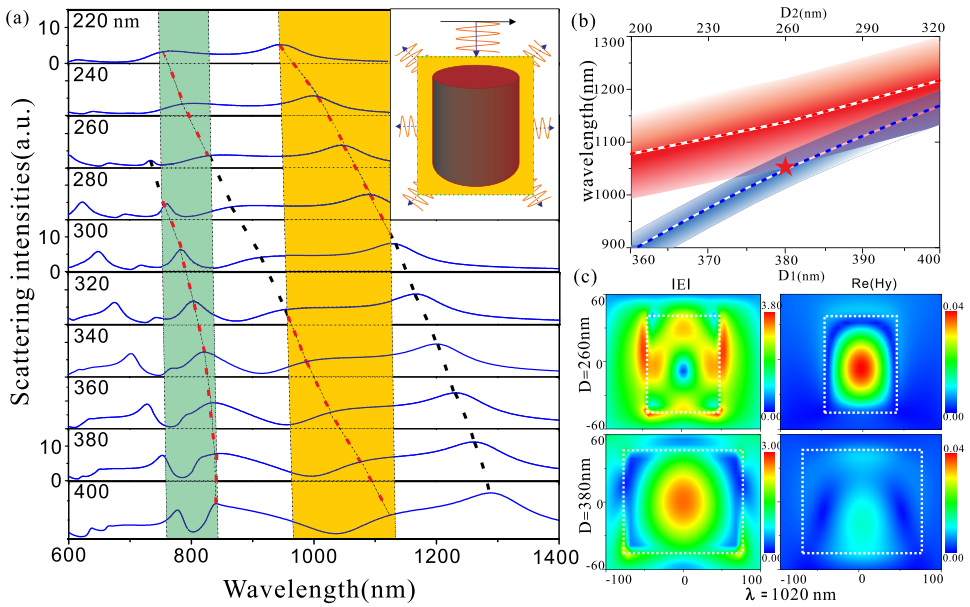

FIG. 1. (a) Calculated scattering intensities of single Si cylinders with different diameters. The diameter increases from 220 nm to 400 nm from top to bottom, with a step size of 20 nm. The positions of the electric or magnetic dipole mode are linked by dotted lines, which are guides to the eye. The green and yellow areas show the wavelength regimes where the different kinds of electromagnetic modes may overlap. The inset shows a schematic diagram of the scattering process of a single cylinder. The linearly polarized light is normally incident onto the system from the top surface of the nanodimer. The blue arrows represent the propagation of the incident light and the scattered light. The black arrow is the polarization of the incident wave. (b) Simulated positions of the electric resonances (red dotted line, corresponding to D1) and the magnetic resonances (blue dotted line, corresponding to D2) as a function of the cylinder diameter. The areas filled with red and blue colors represent the broad electric modes and narrow magnetic modes, which can overlap (area in purple). (c) The cross-sectional electromagnetic-field intensity distributions in the cylinders with diameters of 260 nm and 380 nm at $\lambda = 1020$ nm (marked by the red star in Fig. 1(b)), respectively.

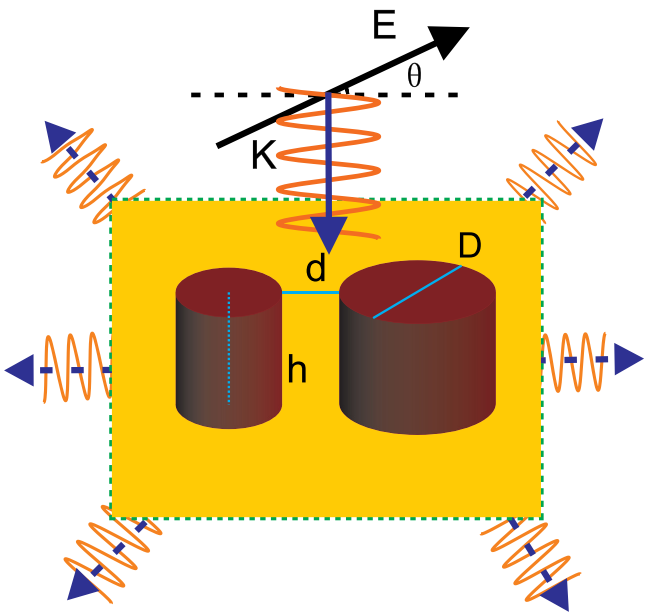

FIG. 2. Schematic diagram of the scattering process of asymmetric Si nanocylinder dimer. The light blue lines measure the three parameters of the structure that we can tune: the gap size of the two cylinders, d; the height of the cylinders, h; and the diameters of the cylinders, D.

should be noted that the polarizabilities are simplified to be scalar in this model. Practically, these polarizabilities should be in tensorial forms, which will be directly applicable to disk geometry.

To consider the interaction between Si nanoparticles, we introduce the coupled electric and magnetic dipole method proposed by Mulholland *et al.*[42] In our system, each particle is regarded as the composition of two dipoles, one electric and the other magnetic. Consequently, the electric and magnetic fields at the *ith* particle induced by the *jth* particle can be written as

$$\begin{cases} \mathbf{E}_i = a_{ij}\alpha_E \mathbf{E}_j + b_{ij}\alpha_E(\mathbf{E}_j \cdot \mathbf{n}_{ji})\mathbf{n}_{ji} - d_{ij}\left(\dfrac{\mu_0}{\varepsilon_0}\right)^{1/2}\chi_H(\mathbf{n}_{ji} \times \mathbf{H}_j) \\ \mathbf{H}_i = a_{ij}\chi_H \mathbf{H}_j + b_{ij}\chi_H(\mathbf{H}_j \cdot \mathbf{n}_{ji})\mathbf{n}_{ji} + d_{ij}\left(\dfrac{\varepsilon_0}{\mu_0}\right)^{1/2}\alpha_E(\mathbf{n}_{ji} \times \mathbf{E}_j), \end{cases} \tag{2}$$

where $\mathbf{n}_{ji}$ denotes the direction vector from the *jth* particle to the *ith* particle. The coefficients a_{ij}, b_{ij}, and d_{ij} from Eqs. (1) and (2) can be expressed as follows:

$$\begin{cases} a_{ij} = \dfrac{1}{4\pi}\dfrac{e^{ikr_{ij}}}{r_{ij}}\left(k^2 - \dfrac{1}{r_{ij}^2} + \dfrac{ik}{r_{ij}}\right) \\ b_{ij} = \dfrac{1}{4\pi}\dfrac{e^{ikr_{ij}}}{r_{ij}}\left(-k^2 + \dfrac{3}{r_{ij}^2} - \dfrac{3ik}{r_{ij}}\right) \\ d_{ij} = \dfrac{1}{4\pi}\dfrac{e^{ikr_{ij}}}{r_{ij}}\left(k^2 + \dfrac{ik}{r_{ij}}\right), \end{cases} \tag{3}$$

where r_{ij} denotes the distance between *ith* and *jth* particles, and $k = 2\pi/\lambda$. Thus, the total induced electric and magnetic dipoles can be derived as

$$\begin{cases} \mathbf{p}_i = \alpha_E\left[\varepsilon_0\mathbf{E}_0 + \sum\limits_{j\neq i} a_{ij}\mathbf{p}_j + b_{ij}(\mathbf{p}_j \cdot \mathbf{n}_{ji})\mathbf{n}_{ji} - (d_{ij}/c)(\mathbf{n}_{ji} \times \mathbf{m}_j)\right] \\ \mathbf{m}_i = \chi_H\left[\mathbf{H}_0 + \sum\limits_{j\neq i} a_{ij}\mathbf{m}_j + b_{ij}(\mathbf{m}_j \cdot \mathbf{n}_{ji})\mathbf{n}_{ji} + d_{ij}c(\mathbf{n}_{ji} \times \mathbf{p}_j)\right], \end{cases} \tag{4}$$

where $c = \sqrt{1/\varepsilon_0\mu_0}$ represents the speed of light in a vacuum. For the case of Si nanoparticles separated by a large distance, the resulting electric and magnetic dipoles can be regarded as equivalent to that of a single nanoparticle because a_{ij}, b_{ij}, $d_{ij} \to 0$ as $r_{ij} \to \infty$. However, in the opposite limit (i.e., $r_{ij} \to 0$), the situation changes dramatically. By calculating the scattering spectra, the interactions between Si nanoparticles can be directly reflected. In fact, according to Eq. (4), three types of interactions among the induced dipoles may occur in the coupled nanoparticles: the electric-to-electric interaction (i.e., $a_{ij}\ \mathbf{p}_j + b_{ij}\ (\mathbf{p}_j \cdot \mathbf{n}_{ji})\ \mathbf{n}_{ji}$ in the induced electric dipoles), the electric-to-magnetic interaction (i.e., $-(d_{ij}/c)(\mathbf{n}_{ji} \times \mathbf{m}_j)$ in the induced electric dipoles and $(d_{ij}\ c)(\mathbf{n}_{ji} \times \mathbf{p}_j)$ in the induced magnetic dipoles), and the magnetic-to-magnetic interaction (i.e., $a_{ij}\ \mathbf{m}_j + b_{ij}(\mathbf{m}_j \cdot \mathbf{n}_{ji})\ \mathbf{n}_{ji}$ in the induced magnetic dipoles).

III. NUMERICAL RESULTS AND DISCUSSION

A. Fano resonances in Si nanocylinder dimer

In order to show how the interaction of electric and magnetic dipoles affects the optical response in the Si nanodimer, we have calculated the optical scattering of the Si nanodimer. Figure 3 shows the scattering spectra and the field distributions of the Si nanodimer. The diameters of the cylinders are 260 nm and 380 nm. From the scattering spectrum in Fig. 3(a), we can see that four obvious peaks emerge in the scattering spectrum. One lies in region A, and the remaining three lie in region B. In this work, we ignore region A and carefully analyze the three peaks in region B (i.e., the infrared regime). We select five positions in the spectrum and label them as I through V. Labels I, III, and V represent the three peaks corresponding to the three resonance locations.

Peak V at $\lambda = 1260$ nm corresponds to the magnetic resonance of the cylinder with a diameter of 380 nm, which can be confirmed by the electric-magnetic field distribution in top panel of Fig. 3(b). That is to say, the dimer exhibits an intense magnetic dipole mode, and there is an obvious enhancement of the scattering light. Thus, peak V is not a Fano resonance peak.

Concerning the Fano resonance peak at $\lambda = 1020$ nm (i.e., peak III), we can clearly observe an annular electric field in the small cylinder corresponding to a strong magnetic field, as well as a strong electric dipole mode inside the big cylinder from the middle panel of Fig. 3(b). Therefore, an intense Fano resonance peak (i.e., peak III) emerges in the scattering spectrum as a result of the coupling of the magnetic and electric modes. Different from the general Fano resonance induced by the coupling of the magnetic dipole mode of the nanoparticle and the electric dipole mode in the gap of nanodimer,[34] this peak mainly relies on the coupling

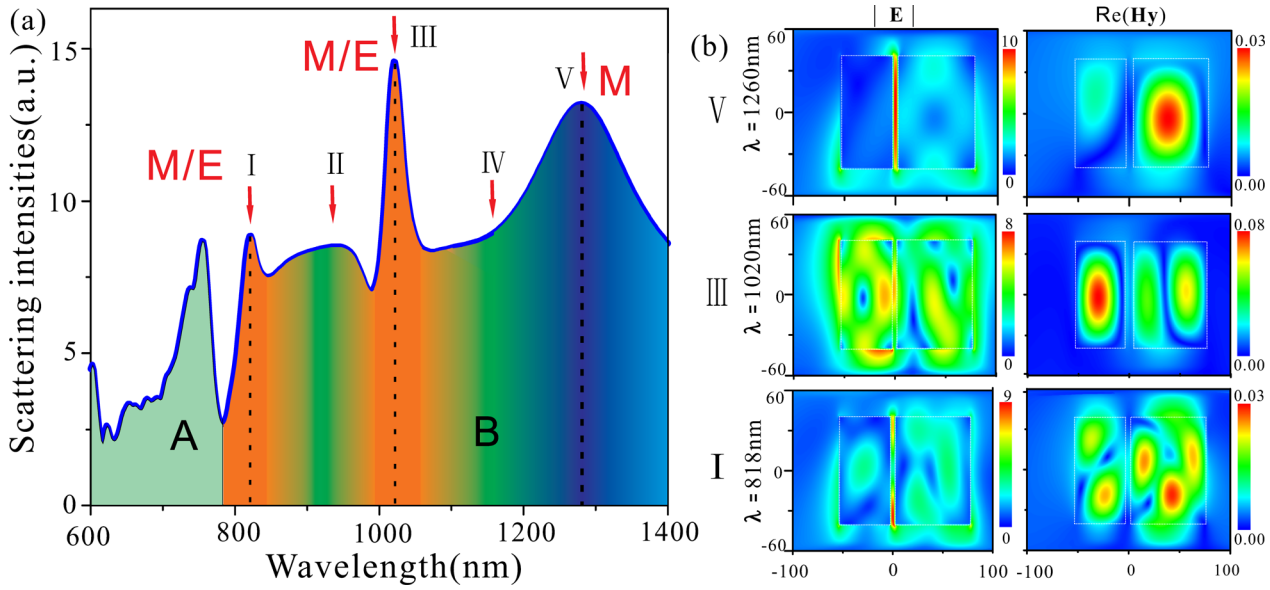

FIG. 3. (a) Calculated scattering intensities of a dimer of Si nanocylinders with diameters of 260 nm and 380 nm. (b) Electric-magnetic field intensity distributions and magnetic field distributions in the x-z plane at $\lambda = 1260$ nm, $\lambda = 1020$ nm, and $\lambda = 818$ nm from top to bottom, with labels decreasing from V to I.

between the magnetic dipole mode in the small cylinder and the electric dipole mode in the big cylinder.

Concerning peak I, which is located at $\lambda = 818$ nm, we can observe an annular magnetic field, which agrees with the electric dipole mode that is exhibited in the electric field distribution inside the small cylinder. In the big cylinder, the magnetic mode becomes excited and interacts with the electric dipole mode of the small one, leading to the second Fano resonance peak I. Furthermore, we also detect the distribution of the modes in the shoulders on the spectrum and pick up two points—peaks II and IV at $\lambda = 958$ nm and $\lambda = 1070$ nm, respectively, where the Fano resonance condition is not well met. In this case, the coupling between the modes naturally becomes less intense, and the peaks do not appear.

B. Polarization-sensitive Fano resonances in Si cylinder dimers

Based on our understanding that the Fano resonances in the Si nanodimer originate from the coupling of the electric dipole in one nanocylinder and the magnetic dipole in the other, it is possible to tune the Fano resonances by changing the polarization of the incident light.

In Fig. 4, as the polarization angle increases from $\theta = 0°$ to $\theta = 90°$, we can see that the Fano resonant peaks at $\lambda = 1020$ nm and $\lambda = 818$ nm gradually fade and disappear, corresponding to an increasingly weaker interaction. On the other hand, at $\lambda = 1058$ nm, there appears an increasingly obvious peak that corresponds to an increasingly intense interaction between the magnetic and electric dipole modes. Moreover, we notice that as the polarization angle increases, a new peak emerges at $\lambda = 946$ nm. To explain the phenomenon, we first check that for a single cylinder, the polarization of the source only has an influence on the orientation of the mode. Even considered in cylinder dimers, each single cylinder exhibits the same main kind of mode; thus the distribution difference is due to the coupling between the modes. The x-z plane section of each field distribution of the electric and magnetic field under sources with different polarizations, namely, $\theta = 0°$, $\theta = 60°$, and $\theta = 90°$ shows what modes exist, as well as the orientation of the modes.

At $\lambda = 1020$ nm, from $\theta = 0°$ to $\theta = 90°$, in the x-z plane we can observe a circularly distributed electric field turning into a two-point distribution in the smaller cylinders, which indicates the orientation change of the magnetic dipole modes. The big cylinder exhibits an annular magnetic field

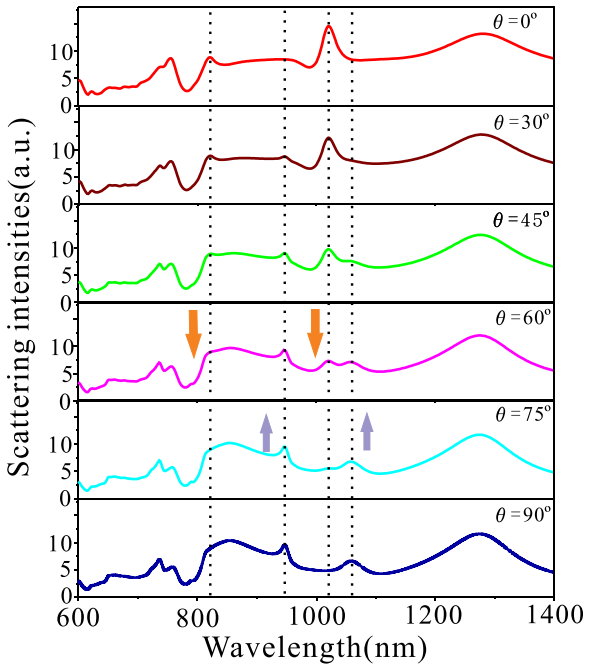

FIG. 4. Calculated scattering intensities of asymmetric Si cylinders dimer with diameters of 260 nm and 380 nm under incident light of different polarizations. From top to bottom, the angle of polarization varies from 0° to 90°. The positions of the peaks are linked by dotted lines. The orange and purple arrows illustrate the fading and increasing peaks, respectively.

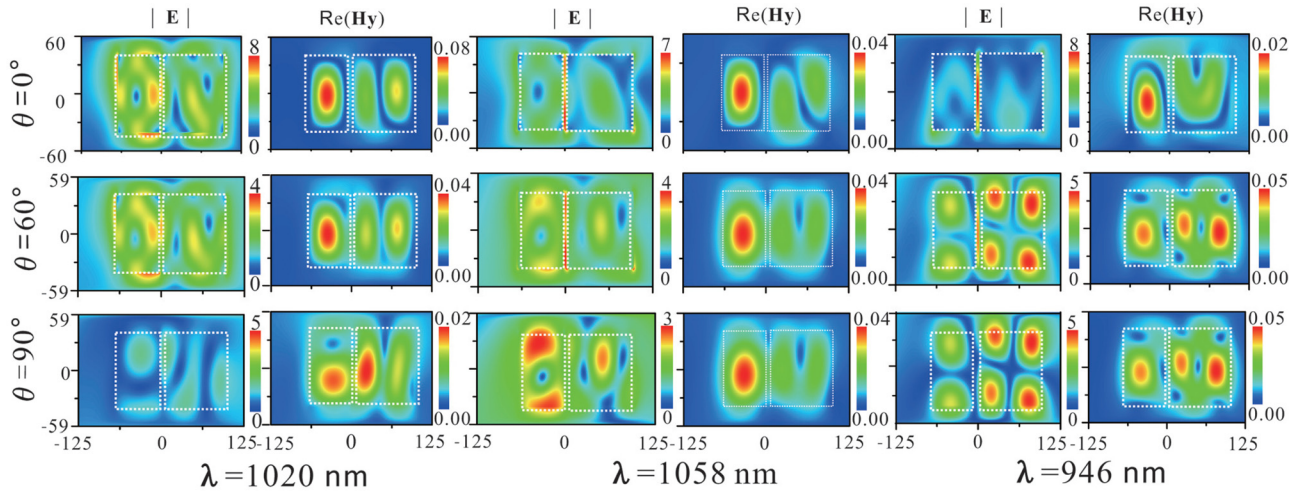

FIG. 5. Each column indicates the calculated electric and magnetic field intensity distributions in the x-z plane at $\lambda = 1020$ nm, $\lambda = 1058$ nm, and $\lambda = 946$ nm, respectively. Each row indicates the polarization angle of the incident light at $\theta = 0°$, $\theta = 60°$, and $\theta = 90°$, respectively.

corresponding to an electric dipole mode. Owing to the orientation change, the overlapping and coupling between the magnetic and electric dipole modes of the cylinders change; these vary from the optimal coupling conditions, which correspond to the highest peak (i.e., the Fano resonance), to the poorest conditions, which correspond to the lower-peak or no-peak situation. The decreasing field intensity around the cylinders for $\lambda = 1020$ nm in Fig. 5 also corresponds to the disappearance of the peaks. However, at $\lambda = 1058$ nm, the increasingly obvious peak simply corresponds to another kind of in-coupling condition between the magnetic and electric dipole modes. The best in-coupling condition is fulfilled when $\theta = 90°$.

Now, we consider the wavelength at $\lambda = 946$ nm. For the smaller cylinder, the x-z plane two-point distributions at $\theta = 60°$ and $\theta = 90°$, combined with the circular distribution at $\theta = 0°$ (which is in fact perpendicular to the distribution of $\theta = 90°$ when without the coupling), indicate that there is mainly a magnetic dipole mode inside the cylinder. On the other hand, for the bigger cylinder, there exists an increasingly obvious coupling-induced hybrid magnetic mode as the polarization angle of the incident light increases, which indicates a new kind of magnetic-magnetic mode coupling.

C. Gap-size-sensitive Fano resonances in Si cylinder dimers

The gap size in the Si nanodimer can influence the coupling of the electric dipole in one nanocylinder and the magnetic dipole in the other. Thus, it is possible to tune the Fano resonances by adjusting the gap distance in this nanosystem. Here, we change the gap distance d between the nanocylinders and measure the wavelength of the most prominent peak around $\lambda = 1020$ nm. Fig. 6 shows the positions of the peaks around 1030 nm as we increase the gap distance between the cylinders from 10 nm to 160 nm. The wavelengths of the peaks have a nearly linear relationship with the gap size of the cylinders, and we obtain the following fitting formula: $\lambda = 1018 + d/10$ (units of nanometers). This indicates a promising method of effectively tuning the position of the Fano resonance in order to realize an accurate wavelength-selective infrared filter.

D. Fano resonances and mode-coupling-induced broadband scattering

It is worthwhile to discuss the broadband optical scattering in the Si nanodimers. Here, we show the scattering features of Si nanodimers with a constant gap size of 20 nm and a height of 240 nm for various diameters of the cylinders.

As shown in Fig. 7, the colored regions represent the span of the broadband scattering. When the diameters of the two cylinders are set to 200 nm and 280 nm, there are two regions corresponding to the broadband scattering (i.e., the red and green areas in the scattering spectrum, fulfilling the half maxima scattering peak requirement). This phenomenon is due to the interference between the electric-magnetic and magnetic-magnetic modes. Not only do the peaks of resonances (i.e., the green area and the peaks of the red area) naturally correspond to a stronger scattering but also the shoulders (e.g., the shoulder of the red area) correspond to weaker coupling of the modes, which makes the scattering band much broader. As the diameters increase, we can see

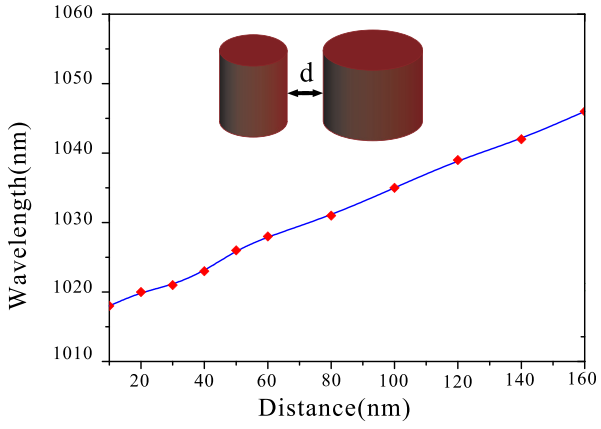

FIG. 6. The calculated resonance wavelength of the Fano effect in the region from 1010 nm to 1060 nm as a function of the gap size d of the cylinders, as illustrated in the inset.

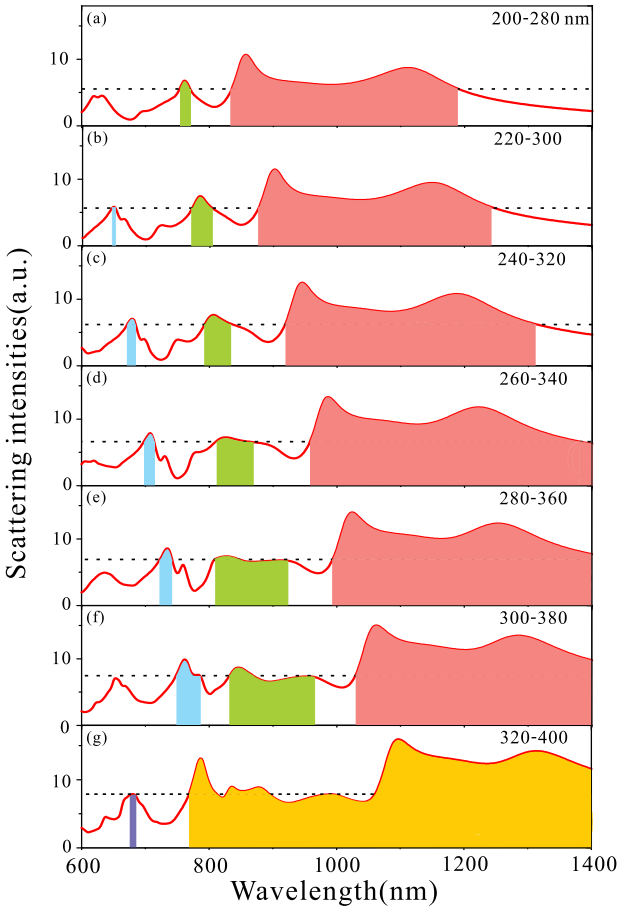

FIG. 7. Calculated scattering intensities of asymmetric Si cylinder dimers with different diameters.

that the red and the green areas become increasingly large (Fig. 7); new regions of blue and purple emerge when the diameters of the dimer are 220 and 300 nm, as well as 320 and 400 nm. The summation of all the areas filled with color becomes increasingly large from Figs. 7(a)–7(f). In particular, for the dimer with diameters of 320 and 400 nm in Fig. 7(g), we can see that the three areas of red, green, and blue almost mix together and, indeed, realize continuous broadband scattering as the yellow area spans from 770 to 1400 nm. Simultaneously, a new purple area appears in the short-wavelength region, thereby indicating a new variety of coupling. Thus, the Si dimer exhibits significant potential for use in high-performance solar cells.

IV. CONCLUSIONS

We have theoretically investigated the optical scattering of a Si nanodimer, which consists of two Si nanocylinders with different diameters. By tuning the relative diameters of the two nanocylinders, dual Fano resonances are found in the Si nanodimer, which originate from the strong coupling between the electric dipole in one nanocylinder and the magnetic dipole in the other. The Fano resonances can be significantly tuned by both adjusting the polarization of the incident light and the gap distance of the nanodimer. Moreover, the intensities of the Fano resonance peaks can be controlled by changing the polarization of the incident light, and the positions of the peaks can also be shifted by varying the gap distance. Additionally, the Si nanodimer exhibits a broadband scattering response, which originates from the electric-magnetic and magnetic-magnetic coupling between the modes of the nanocylinders. These results concerning the loss-less, easily fabricated Si nanodimer may have promising applications in infrared filters, solar cells, biosensing. And similar phenomena can be found in the microwave region[43,44] and benefit the application to metamaterials.

ACKNOWLEDGMENTS

This work was supported by the Ministry of Science and Technology of China (Grant No. 2012CB921502), and the National Natural Science Foundation of China (Grant Nos. 61475070, 11474157, 11321063, and 91321312).

[1]U. Fano, Phys. Rev. **124**, 1866 (1961).
[2]A. E. Miroshnichenko, S. Flach, and Y. S. Kivshar, Rev. Mod. Phys. **82**, 2257 (2010).
[3]B. Luk'yanchuk, N. I. Zheludev, S. A. Maier, N. J. Halas, P. Nordlander, H. Giessen, and C. T. Chong, Nat. Mater. **9**, 707 (2010).
[4]N. J. Halas, S. Lal, W. S. Chang, S. Link, and P. Nordlander, Chem. Rev. **111**, 3913 (2011).
[5]Y. J. Bao, R. W. Peng, D. J. Shu, M. Wang, X. Lu, J. Shao, W. Lu, and N. B. Ming, Phys. Rev. Lett. **101**, 087401 (2008).
[6]K. Zhang, C. Wang, L. Qin, R. W. Peng, D. H. Xu, X. Xiong, and M. Wang, Opt. Lett. **39**, 3539 (2014).
[7]L. Qin, K. Zhang, R. W. Peng, X. Xiong, W. Zhang, X. R. Huang, and M. Wang, Phys. Rev. B **87**, 125136 (2013).
[8]F. Hao, P. Nordlander, Y. Sonnefraud, P. V. Dorpe, and S. A. Maier, ACS Nano **3**, 643 (2009).
[9]Y. H. Fu, J. B. Zhang, Y. F. Yu, and B. Luk'yanchuk, ACS Nano **6**, 5130 (2012).
[10]F. López-Tejeiral, R. Paniagua-Domínguez, R. Rodríguez-Oliveros, and J. A. Sánchez-Gil, New J. Phys. **14**, 023035 (2012).
[11]J. B. Lassiter, H. Sobhani, J. A. Fan, J. Kundu, F. Capasso, P. Nordlander, and N. J. Halas, Nano Lett. **10**, 3184 (2010).
[12]S. D. Liu, Z. Yang, R. P. Liu, and X. Y. Li, ACS Nano **6**, 6260 (2012).
[13]S. Mukherjee, H. Sobhani, J. B. Lassiter, R. Bardhan, P. Nordlander, and N. J. Halas, Nano Lett. **10**, 2694 (2010).
[14]H. J. Chen, L. Shao, Y. C. Man, C. M. Zhao, J. F. Wang, and B. C. Yang, Small **8**, 1503 (2012).
[15]D. J. Wu, S. M. Jiang, and X. J. Liu, J. Phys. Chem. C **115**, 23797 (2011).
[16]G. Bachelier, I. Russier-Antoine, E. Benichou, C. Jonin, N. Del Fatti, F. Vallée, and P. F. Brevet, Phys. Rev. Lett. **101**, 197401 (2008).
[17]A. E. Cetin and H. Altug, ACS Nano **6**, 9989 (2012).
[18]A. H. Safavi-Naeini, T. P. M. Alegre, J. Chan, M. Eichenfield, M. Winger, Q. Lin, J. T. Hill, D. E. Chang, and O. Painter, Nature **472**, 69 (2011).
[19]S. L. Chua, Y. Chong, A. D. Stone, M. Soljacic, and J. Brovo-Abad, Opt. Express **19**, 1539 (2011).
[20]J. A. Fan, C. Wu, K. Bao, J. M. Bao, R. Bardhan, N. J. Halas, V. N. Manoharan, P. Nordlander, G. Shvets, and F. Capasso, Science **328**, 1135 (2010).
[21]W. Zhang, A. O. Govorov, and G. W. Bryanfangt, Phys. Rev. Lett. **97**, 146804 (2006).
[22]B. Tang, L. Dai, and C. Jiang, Opt. Express **19**, 628 (2011).
[23]V. A. Fedotov, A. Tsiatmas, J. H. Shi, R. Buckingham, P. de Groot, Y. Chen, S. Wang, and N. I. Zheludev, Opt. Express **18**, 9015 (2010).
[24]Q. Zhao, J. Zhou, F. Zhang, and D. Lippens, Mater. Today **12**, 60 (2009).
[25]P. Albella, M. A. Poyli, M. K. Schmidt, S. A. Maier, F. Moreno, J. J. Saénz, and J. Aizpurua, J. Phys. Chem. C **117**, 13573 (2013).
[26]G. Boudarham, R. Abdeddaim, and N. Bonod, Appl. Phys. Lett. **104**, 021117 (2014).
[27]A. Mirzaei and A. E. Miroshnichenko, Nanoscale **7**, 5963 (2015).
[28]R. M. Bakker, D. Permyakov, Y. F. Yu, D. Markovich, R. Paniagua-Domłnguez, L. Gonzaga, A. Samusev, Y. Kivshar, B. Lukyanchuk, and A. I. Kuznetsov, Nano Lett. **15**, 2137 (2015).

[29]B. Hopkins, D. S. Filonov, A. E. Miroshnichenko, F. Monticone, A. Alu, and Y. S. Kivshar, ACS Photonics **2**, 724 (2015).
[30]A. E. Miroshnichenko and Y. S. Kivshar, Nano Lett. **12**, 6459 (2012).
[31]D. S. Filonov, A. P. Slobozhanyuk, A. E. Krasnok, P. A. Belov, E. A. Nenasheva, B. Hopkins, and Y. S. Kivshar, Appl. Phys. Lett. **104**, 021104 (2014).
[32]K. E. Chong, B. Hopkins, I. Staude, A. E. Miroshnichenko, J. Dominguez, M. Decker, and Y. S. Kivshar, Small **10**, 1985 (2014).
[33]M. Pu, M. Song, H. Yu, C. Hu, M. Wang, X. Wu, and X. Luo, Appl. Phys. Express **7**, 032002 (2014).
[34]J. Yan, P. Liu, Z. Lin, H. Wang, H. Chen, C. Wang, and G. Yang, ACS Nano **9**, 2968 (2015).
[35]M. C. Cassidy, H. R. Chan, B. D. Ross, P. K. Bhattacharya, and C. M. Marcus, Nat. Nanotechnol. **8**, 363 (2013).
[36]U. Zywietz, A. B. Evlyukhin, C. Reinhardt, and B. N. Chichkov, Nat. Commun. **5**, 3402 (2014).
[37]C. Wang, Z. Y. Jia, K. Zhang, Y. Zhou, R. H. Fan, X. Xiong, and R. W. Peng, J. Appl. Phys. **115**, 244312 (2014).
[38]B. Tian, X. Zheng, T. J. Kempa, Y. Fang, N. F. Yu, G. H. Yu, J. L. Huang, and C. M. Lieber, Nature **449**, 885 (2007).
[39]L. H. Zhu, M. R. Shao, R. W. Peng, R. H. Fan, X. R. Huang, and M. Wang, Opt. Express **21**, A313 (2013).
[40]I. Staude, A. E. Miroshnichenko, M. Decker, N. T. Fofang, S. Liu, E. Gonzales, J. Domingue, T. S. Luk, D. N. Neshev, I. Brener, and Y. Kivshar, ACS Nano **7**, 7824 (2013).
[41]A. B. Evlyukhin, C. Reinhardt, and B. N. Chichkov, Phys. Rev. B **84**, 235429 (2011).
[42]G. W. Mulholland, C. F. Bohren, and K. A. Fuller, Langmuir **10**, 2533 (1994).
[43]I. Vendik, O. Vendik, and M. Odit, Microwave Opt. Technol. Lett. **48**, 2553 (2006).
[44]I. B. Vendik, M. A. Odit, and D. S. Kozlov, Metamaterial **3**, 140 (2009).